

# Horizon-Evanescent Scalar Clouds from Coupled Rotation and Magnetic Fields around Black Holes

Hengyu Xu,<sup>1,2,\*</sup> Haowei Chen,<sup>1,2,†</sup> and Shao-Jun Zhang<sup>1,2,‡</sup>

<sup>1</sup>*Institute for Theoretical Physics and Cosmology,  
Zhejiang University of Technology, Hangzhou 310032, China*

<sup>2</sup>*School of Physics and Optical Engineering,  
Zhejiang University of Technology, Hangzhou 310032, China*

(Dated: July 10, 2026)

We show that black-hole rotation and an external magnetic field can jointly generate a qualitatively new class of scalar cloud. Using the Kerr-Bertotti-Robinson geometry as a separable laboratory for magnetized rotating black holes, we study a charged massive scalar field and map the radial Klein-Gordon equation into a one-dimensional Schrödinger-like form. The magnetic coupling shifts the near-horizon dispersion relation and realizes a positive horizon gap: a sufficient near-horizon criterion under which the horizon wavenumber becomes purely imaginary in a finite frequency band below the usual kinematic synchronization frequency. In this band the physical horizon boundary condition is no longer a propagating ingoing wave, but a regular exponentially decaying state. This rotation-magnetic-field mechanism quenches the superradiant flux and supports horizon-decaying scalar clouds (Type-II), distinct from the usual synchronized propagating clouds (Type-I). Matched asymptotic expansions and numerical shooting solutions are used to exhibit both branches and their spatial profiles. Thus the Kerr-Bertotti-Robinson solution is not an isolated curiosity, but an explicit realization of a broader positive-gap criterion for stationary bosonic configurations absent in isolated Kerr systems.

## I. INTRODUCTION

The extraction of rotational energy from a black hole is one of the most fascinating predictions of general relativity, initially conceptualized by Penrose [1–3]. In the realm of wave dynamics, this energy extraction manifests as superradiance. When a bosonic wave impinges on a rotating black hole, it can be amplified if its frequency  $\omega$  satisfies the superradiant condition  $0 < \omega < m\Omega_H$ , where  $m$  is the azimuthal quantum number and  $\Omega_H$  is the angular velocity of the black hole horizon [4–9].

---

\* xuhengyu0501@outlook.com

† chenhaowei@zjut.edu.cn

‡ sjzhang@zjut.edu.cn (corresponding author)

If the bosonic field possesses a non-zero rest mass  $\mu_s$ , the mass term acts as a natural effective mirror at spatial infinity, trapping the amplified low-frequency modes in the vicinity of the black hole [10]. This geometric confinement leads to a continuous, exponentially growing extraction of energy, triggering the well-known superradiant instability, often referred to as the “black hole bomb” mechanism [11–14]. Over the decades, the massive scalar field instability has been thoroughly investigated through analytical matching techniques and precise numerical methods across various regimes of the parameter space [15–18]; see Ref. [19] for a comprehensive review.

At the exact threshold of this superradiant instability ( $\omega = m\Omega_H$  in Kerr, or its charged generalization in Kerr-Newman), the net energy flux across the event horizon strictly vanishes. In this highly tuned kinematic regime, the massive field does not grow or decay, but instead forms a completely stationary, non-dissipative bound state. These long-lived configurations, famously known as “scalar clouds,” have been extensively studied in standard Kerr and Kerr-Newman spacetimes [20–23]. They represent the linear onset of black hole scalar hair, challenging the traditional no-hair paradigm and providing profound insights into the non-linear dynamics of fields in curved spacetimes [24–26]. Analogous bound-state phenomena have also been explored for vector and tensor fields [27–29], as well as in acoustic black hole analogues [30, 31]. In all these familiar cases, however, the zero-flux cloud is still obtained as the synchronized limit of a propagating horizon wave. The possibility that a stationary cloud may instead be supported by an evanescent, horizon-decaying boundary condition has not been systematically explored.

However, realistic astrophysical black holes do not exist in isolation; they are typically surrounded by accretion disks and diffuse plasmas that generate strong external magnetic fields [32, 33]. The presence of an external magnetic field significantly alters both the spacetime geometry and the effective interactions of any charged fields propagating within it. Traditionally, the exact solutions describing rotating black holes immersed in strong magnetic universes have been constructed via the Ernst formulation [34], which relies on the Melvin magnetic universe [35]. The thermodynamic and geometric properties of such magnetized rotating black holes exhibit profound deviations from asymptotic flatness, introducing complex ergoregion structures and altered horizon topologies [36–40]. Naturally, this exact framework has been the primary arena for investigating how magnetic fields affect superradiant instabilities. Studies of wave dynamics in Ernst-type backgrounds have revealed intricate couplings between the field’s charge and the external magnetic potential, demonstrating that magnetic fields can dynamically enhance or suppress superradiance [41–43], and explicitly supporting the existence of stationary scalar clouds in Melvin-Kerr spacetimes [44].

Despite these analytical successes, investigating wave dynamics in the Ernst formulation poses a fundamental mathematical challenge: the standard magnetized Kerr solution generally loses the algebraic Type D classification of the original isolated Kerr metric. This loss of algebraic symmetry severely complicates the exact separability of the Klein-Gordon and Teukolsky equations, often forcing analyses of scalar clouds to rely on stringent weak-field limits, extreme spin assumptions, or specialized numerical approximations. To address this mathematical bottleneck and study magnetized scalar clouds in a more geometrically tractable framework, one can turn to alternative exact solutions of the Einstein-Maxwell equations.

Recently, Podolský and Ovcharenko formulated a new class of exact spacetimes—the Kerr-Bertotti-Robinson (Kerr-BR) black holes [45–47], whose rigorous thermodynamic properties, conserved charges, and first law of black-hole thermodynamics have also been recently established [48]. In the present work, we use this geometry primarily as a controlled theoretical laboratory for isolating how rotation and a magnetic field act together on scalar-field boundary conditions. To build physical intuition, it is useful to distinguish this exact geometry from the well-known Wald solution [33]. While the Wald solution merely superimposes a test magnetic field onto a standard asymptotically flat Kerr vacuum, the Kerr-BR metric fully incorporates the non-linear gravitational backreaction of the electromagnetic field. Consequently, its asymptotic structure does not reduce to flat space, but naturally approaches the Bertotti-Robinson universe—a geometry intrinsically supported by a uniform magnetic field. Furthermore, unlike the Ernst-magnetized models, this spacetime successfully retains the algebraic Type D classification while describing a Kerr black hole immersed in an asymptotically uniform magnetic field with non-aligned principal null directions. This algebraic structure makes the weak-field separable sector especially useful for identifying mechanisms that would otherwise be obscured by non-separability.

In this paper, we systematically investigate the dynamics of a massive charged scalar field in the weak-field separable sector of the Kerr-BR spacetime. The central result is a rotation–magnetic-field mechanism for producing a second, horizon-decaying class of scalar cloud. The rotation supplies the usual superradiant channel through the azimuthal coupling to the horizon angular velocity, while the magnetic field dresses both the asymptotic confinement and the near-horizon dispersion relation of the charged scalar. Their combined effect creates a finite frequency interval in which the mode remains below the kinematic synchronization frequency, but the effective radial wavenumber at the horizon becomes imaginary. The horizon boundary condition therefore changes from a propagating ingoing wave to a regular evanescent state. Through matched asymptotic expansions using confluent hypergeometric functions [49, 50], we show that this transition quenches

the superradiant flux and removes the dissipative imaginary part of the bound-state frequency.

Consequently, the usual synchronized scalar clouds appear here as Type-I states located at the lower boundary of the propagating branch, whereas the main new branch consists of Type-II scalar clouds that exponentially decay toward the event horizon. Supported by numerical shooting integrations [51], we show that these Type-II clouds have a near-horizon structure that is qualitatively different from the plateau behavior of the synchronized clouds.

The main message of this work can be summarized in three points. First, the zero-flux condition for a scalar cloud need not arise only from synchronization of a propagating horizon wave. Second, in a magnetized rotating geometry the combined rotational and electromagnetic couplings can open a positive near-horizon gap, turning the horizon channel into an evanescent one. Third, once this evanescent branch is combined with confinement at infinity, it supports a stationary scalar cloud whose horizon behavior is qualitatively different from the familiar Kerr and Kerr-Newman clouds. In this sense, the Kerr-BR spacetime is not the end point of the analysis, but a clean realization of a more general positive-gap criterion: whenever the separated near-horizon radial equation contains a positive gap term, an evanescent scalar-cloud branch becomes possible.

The paper is organized to emphasize this mechanism. In Sec. II, we introduce the Kerr-BR spacetime as a tractable magnetized rotating background and derive the scalar-field equation. In Sec. III, we map the radial equation into a Schrödinger-like form, derive the horizon gap, and state a general criterion for horizon-evanescent clouds. Sec. IV presents the analytic bound-state argument for the rotation–magnetic quenching mechanism. In Sec. V, we present numerical shooting results that distinguish the propagating Type-I reference clouds from the horizon-decaying Type-II clouds. Finally, we conclude in Sec. VI.

## II. A TRACTABLE MAGNETIZED ROTATING BACKGROUND

To investigate the rotation–magnetic-field mechanism in a setting where the scalar equation remains analytically tractable, we consider a Kerr black hole immersed in an external uniform magnetic field, described by the Kerr-Bertotti-Robinson or Kerr-BR spacetime [45]. The metric has a compact explicit form

$$ds^2 = \frac{1}{\Omega^2} \left[ -\frac{Q}{\rho^2} (dt - a \sin^2 \theta d\varphi)^2 + \frac{\rho^2}{Q} dr^2 + \frac{\rho^2}{P} d\theta^2 + \frac{P}{\rho^2} \sin^2 \theta (a dt - (r^2 + a^2) d\varphi)^2 \right], \quad (1)$$

where the metric functions are given by

$$\begin{aligned}
\rho^2 &= r^2 + a^2 \cos^2 \theta, \\
P &= 1 + B^2 \left( M^2 \frac{I_2}{I_1^2} - a^2 \right) \cos^2 \theta, \\
Q &= (1 + B^2 r^2) \Delta, \\
\Omega^2 &= (1 + B^2 r^2) - B^2 \Delta \cos^2 \theta,
\end{aligned} \tag{2}$$

with the horizon function  $\Delta = \left( 1 - B^2 M^2 \frac{I_2}{I_1^2} \right) r^2 - 2M \frac{I_2}{I_1} r + a^2$ . Here,  $M$  and  $a$  represent the mass and specific angular momentum of the black hole, respectively, and  $B$  denotes the magnetic field strength. The constants are  $I_1 = 1 - \frac{1}{2} B^2 a^2$  and  $I_2 = 1 - B^2 a^2$ .

The electromagnetic field is given by the complex 1-form potential (its real counterpart is  $A^{\text{real}} \equiv 2 \text{Re } A$ ):

$$A = \frac{e^{i\xi}}{2B} \left[ \Omega_{,r} \frac{a dt - (r^2 + a^2) d\varphi}{r + ia \cos \theta} + \frac{i\Omega_{,\theta}}{\sin \theta} \frac{dt - a \sin^2 \theta d\varphi}{r + ia \cos \theta} + (\Omega - 1) d\varphi \right], \tag{3}$$

which clearly vanishes for  $B = 0$ .

The propagation of a massive, charged test scalar field  $\Phi$  with mass  $\mu_s$  and charge  $q$  is governed by the covariant Klein-Gordon (KG) equation:

$$[(\nabla_\mu - iqA_\mu)(\nabla^\mu - iqA^\mu) - \mu_s^2] \Phi = 0. \tag{4}$$

When the magnetic field is weak ( $B \ll 1$ ), we explicitly take the electromagnetic phase parameter to be  $\xi = 0$ , which represents the pure magnetic field. We work in the weak-field separable sector of the geometry, retaining the leading magnetic couplings that enter the charged scalar dynamics while keeping the radial and angular equations decoupled. This controlled limit is sufficient for isolating the rotation–magnetic mechanism responsible for the new horizon boundary condition. Under this condition, substituting the separable ansatz  $\Phi(t, r, \theta, \phi) = \sum_{l,m} e^{i(m\phi - \omega t)} R(r) S(\theta)$  into the field equation allows us to derive the radial and angular equations. The complete forms of these equations, including the magnetic-field and scalar-charge couplings kept in this approximation, are detailed in Appendix A.

### III. NEAR-HORIZON MECHANISM AND GENERAL CRITERION

#### A. Schrödinger-like Radial Equation in Tortoise Coordinates

To analyze the physical boundary conditions, we map the radial equation into a one-dimensional Schrödinger-like form. We introduce the tortoise coordinate  $y$ , mapping the exterior domain  $r \in$

$(r_+, \infty)$  to  $y \in (-\infty, +\infty)$ , defined by  $dy/dr = (r^2 + a^2)/\Delta_0(r)$ , where  $\Delta_0(r) = r^2 - 2Mr + a^2$ . Here,  $r_{\pm} = M \pm \sqrt{M^2 - a^2}$  denote the outer and inner horizons, respectively.

By redefining the radial wave function as  $Y = \sqrt{r^2 + a^2} R$ , the radial equation is cast into:

$$\frac{d^2 Y(y)}{dy^2} - V_{\text{eff}}(y; \omega, \mu_s, B, q, a) Y(y) = 0. \quad (5)$$

The properties of the bound states are completely dictated by the asymptotic behavior of  $V_{\text{eff}}$ .

## B. Asymptotic Behavior and Physical Boundary Conditions

**Spatial Infinity** ( $y \rightarrow +\infty, r \rightarrow \infty$ ): Far from the black hole, the effective potential approaches  $k_f^2 \equiv Bmq + \mu_s^2 - 2aBq\omega - \omega^2$ . In this asymptotic limit, the combination  $\mu_{\text{eff}}^2 \equiv \mu_s^2 + Bmq - 2aBq\omega$  perfectly plays the role of an effective scalar mass squared, which is dynamically dressed by the external magnetic field. To investigate localized scalar clouds, we demand  $k_f^2 = \mu_{\text{eff}}^2 - \omega^2 > 0$ , imposing the bound-state requirement:  $Y(y \rightarrow +\infty) \sim e^{-k_f y}$ .

To satisfy  $k_f^2 > 0$ , the bare scalar mass  $\mu_s$  must be sufficiently large to counteract any repulsive effects from the magnetic coupling. While the complete piecewise constraints across all signs of  $B$ ,  $q$ , and  $m$  are collected in Appendix B, the underlying physics becomes highly intuitive for the most relevant superradiant regime ( $m > 0, a > 0$ ). As summarized in Table I, when the magnetic field and scalar charge are aligned ( $Bq > 0$ ), the magnetic dressing enhances confinement, allowing even massless fields ( $\mu_s \geq 0$ ) to form bound states. Conversely, an anti-aligned configuration ( $Bq < 0$ ) effectively reduces the scalar mass, thus necessitating a strict minimum bare mass cut-off to maintain wave confinement at spatial infinity.

TABLE I. Bound-state parameter constraints for the physically relevant superradiant regime ( $m > 0, a > 0$ ). The field-charge alignment ( $Bq$ ) dictates the minimum bare scalar mass ( $\mu_s$ ) required for wave confinement. The exhaustive piecewise conditions for all  $m, B, q$  limits are preserved in Appendix B.

Field-Charge Alignment	Azimuthal Mode ( $m > 0$ )	Minimum Bare Mass ( $\mu_s$ )
$Bq > 0$ (Aligned)	All $m > 0$	$\mu_s \geq 0$
$Bq = 0$ (Neutral/No Field)	All $m > 0$	$\mu_s > 0$
$Bq < 0$ (Anti-aligned)	$0 < m \leq -a^2 Bq$	$\mu_s \geq 0$
$Bq < 0$ (Anti-aligned)	$m > -a^2 Bq$	$\mu_s \geq \sqrt{-a^2 B^2 q^2 - Bmq}$

**Event Horizon** ( $y \rightarrow -\infty, r \rightarrow r_+$ ): Near the horizon, the effective potential asymptotes to  $-k_h^2 \equiv -[(\omega - \omega_c)^2 - (\omega_c^2 - D)]$ , where  $\omega_c = m\Omega_H + q\Phi_H = ma/(2Mr_+) - aBqr_+/(4M)$  is the modified superradiant threshold frequency evaluated at the event horizon, with  $\Omega_H$  and  $\Phi_H$  being the angular velocity and electromagnetic potential at the horizon, respectively. The zeroes of the horizon wavenumber,  $\omega_1 = \omega_c - \sqrt{\omega_c^2 - D}$  and  $\omega_2 = \omega_c + \sqrt{\omega_c^2 - D}$ , serve as critical phase-transition boundaries. The parameter  $D$  captures the non-linear coupling:

$$D = -\frac{a^4 Bmq + 2m^2 M \left( \sqrt{M^2 - a^2} - M \right) + a^2 m^2}{4a^2 M^2}. \quad (6)$$

To demonstrate the existence of this quenching band, we evaluate the discriminant  $\omega_c^2 - D$ . Substituting the explicit expressions for  $\omega_c$  and  $D$ , we obtain:

$$\omega_c^2 - D = \frac{a^2 B^2 q^2 \left[ a^4 - 4a^2 M \left( \sqrt{M^2 - a^2} + 2M \right) + 8M^3 \left( \sqrt{M^2 - a^2} + M \right) \right]}{16M^2 \left( \sqrt{M^2 - a^2} + M \right)^2}. \quad (7)$$

The polynomial term in the square brackets factors as  $(M + \sqrt{M^2 - a^2})^4 = r_+^4$ . Recognizing that the denominator contains  $16M^2 r_+^2$ , the expression simplifies to

$$\omega_c^2 - D = \frac{a^2 B^2 q^2 r_+^2}{16M^2} > 0. \quad (8)$$

For nonzero  $a$ ,  $B$ , and  $q$ , this discriminant is positive. The critical phase-transition frequencies  $\omega_1$  and  $\omega_2$  are therefore real, and the quenching band  $[\omega_1, \omega_2]$  exists in the physical parameter space considered here.

### C. Physical Horizon Boundary Condition

The physical meaning of this band is fixed by the boundary condition at the future event horizon. A local observer just outside the horizon is dragged with angular velocity  $\Omega_H$ . Including the electromagnetic coupling, the near-horizon phase of a charged scalar mode is

$$\psi \sim e^{-i(\omega - m\Omega_H - q\Phi_H)t} e^{\pm ik_h y} = e^{-i(\omega - \omega_c)t} e^{\pm ik_h y}. \quad (9)$$

For  $k_h^2 > 0$ , the horizon channel is propagating. The sign of the spatial phase is then chosen so that the wave is ingoing in the locally nonrotating frame [52]. Thus the usual superradiant regime requires both the kinematic condition  $0 < \omega < \omega_c$  and a real horizon wavenumber. In the present system these two requirements do not define the same interval: the propagating superradiant branch ends at  $\omega_1$ , not at  $\omega_c$ .

For  $\omega_1 < \omega < \omega_2$ , however,  $k_h^2 < 0$  and the horizon channel is no longer propagating. Writing  $k_h = -i\kappa_h$  with  $\kappa_h > 0$ , the regular solution is

$$Y \sim e^{\kappa_h y}, \quad y \rightarrow -\infty, \quad (10)$$

which decays toward the event horizon. Its conserved radial flux,

$$\mathcal{F}_H \propto \frac{1}{2i} \left( Y^* \frac{dY}{dy} - Y \frac{dY^*}{dy} \right), \quad (11)$$

vanishes identically for the real exponential boundary condition. The quenching of superradiance is therefore not merely the usual synchronization condition; it is a change in the horizon channel itself, from a propagating wave to an evanescent state. This is the boundary-condition origin of the Type-II clouds.

#### D. A General Criterion for Horizon-Decaying Clouds

The above result also suggests a useful near-horizon criterion for when the same mechanism can appear in other magnetized rotating black holes. Consider a stationary and axisymmetric magnetized black-hole background with horizon generator

$$\chi = \partial_t + \Omega_H \partial_\varphi, \quad (12)$$

and horizon electrostatic potential

$$\Phi_H \equiv -\chi^\mu A_\mu|_{r=r_+}. \quad (13)$$

For a charged scalar mode

$$\Phi \sim e^{-i\omega t + im\varphi} S(\theta) R(r), \quad (14)$$

the kinematic synchronization frequency is always

$$\omega_c = m\Omega_H + q\Phi_H. \quad (15)$$

Suppose that, after separation and a regular near-horizon field redefinition, the radial equation can be written near the horizon as

$$\frac{d^2 Y}{dy^2} + k_h^2 Y = 0, \quad k_h^2 = (\omega - \omega_c)^2 - \mathcal{G}_H, \quad (16)$$

where  $y \rightarrow -\infty$  at the horizon and  $\mathcal{G}_H$  is a real horizon gap generated by the magnetic and rotational couplings. In ordinary Kerr or Kerr-Newman backgrounds,  $\mathcal{G}_H = 0$ , so the only zero-flux scalar cloud occurs at the synchronization point  $\omega = \omega_c$ . By contrast, if a magnetized rotating black hole has

$$\mathcal{G}_H > 0, \quad (17)$$

then the horizon wavenumber is imaginary in the finite interval

$$\omega_c - \sqrt{\mathcal{G}_H} < \omega < \omega_c + \sqrt{\mathcal{G}_H}. \quad (18)$$

The two endpoints are the analogues of  $\omega_1$  and  $\omega_2$ . Inside this interval the regular radial solution is

$$Y \sim e^{\kappa_H y}, \quad \kappa_H = \sqrt{\mathcal{G}_H - (\omega - \omega_c)^2}, \quad (19)$$

which decays toward the future event horizon. Since this boundary condition is a real exponential rather than a traveling wave, the same conserved radial current used in Eq. (11) gives no net horizon transport. Therefore the superradiant energy exchange is quenched not by kinematic synchronization alone, but by the conversion of the horizon channel from propagating to evanescent. If the same mode is also confined at infinity, the usual bound-state quantization then yields a stationary horizon-decaying scalar cloud.

In the Kerr-BR weak-field sector studied here, Eq. (16) is realized with

$$\mathcal{G}_H = \omega_c^2 - D = \frac{a^2 B^2 q^2 r_+^2}{16M^2}. \quad (20)$$

Thus the gap vanishes whenever the rotation, magnetic field, or scalar charge is removed, and the Type-II branch collapses back to the usual synchronized-cloud picture. This shows that the horizon-decaying clouds found below are not an artifact of notation, but a concrete realization of a broader criterion: a positive rotation–magnetic horizon gap is sufficient to generate an evanescent scalar-cloud branch.

The important point is that the sign of  $k_h^2$  is controlled by the joint appearance of rotation and magnetic coupling in  $\omega_c$  and  $D$ . Depending on this sign, the near-horizon boundary condition bifurcates into two distinct branches:

- **Propagating Branch** ( $k_h^2 > 0$ ): The wave is physically ingoing,  $Y \sim e^{ik_h y}$  for  $0 < \omega < \omega_1$ , permitting rotational energy extraction (superradiance).

- **Horizon-Evanescent Branch** ( $k_h^2 < 0$ ): The horizon wavenumber becomes imaginary,  $k_h = -i\kappa_h$ . The regular solution exponentially decays toward the horizon,  $Y \sim e^{\kappa_h y}$ . This is the branch that gives rise to Type-II scalar clouds.

### E. Classification of Bound States

Defining the asymptotic cutoff frequency as  $\omega_f = -aBq + \sqrt{Bmq + a^2B^2q^2 + \mu_s^2}$ , the bound states naturally divide into three regimes:

1. **Superradiant bound states** ( $0 < \omega < \min\{\omega_1, \omega_f\}$ ):  $k_h^2 > 0$ . The wave is propagating at the horizon and extracts rotational energy.
2. **Horizon-decaying bound states** ( $\omega_1 \leq \omega \leq \min\{\omega_2, \omega_f\}$ ):  $k_h^2 \leq 0$ . The joint rotational and magnetic couplings convert the horizon behavior into an evanescent decay,  $Y \sim e^{\kappa_h y}$ , quenching the superradiant flux.
3. **Non-superradiant bound states** ( $\omega_2 < \omega < \omega_f$ ):  $k_h^2 > 0$  but  $\omega > \omega_c$ . The wave is again propagating at the horizon, now in the absorbing regime.

## IV. ANALYTIC BOUND-STATE SPECTRUM AND ROTATION–MAGNETIC QUENCHING

The transition from a propagating to an exponentially decaying horizon boundary condition alters the fundamental nature of the bound states. Employing the matched asymptotic expansion method [13], we analytically map the complex frequency

$$\omega = \omega^{(0)} + \delta\omega. \quad (21)$$

Appendix C gives the technical expansion of the special functions. Here we present the essential derivation because it is the analytic core of the Type-II mechanism.

In the far region,  $r \gg M$ , the radial equation reduces to a Coulomb-type bound-state equation. With

$$k^2 = \omega^2 - \mu_s^2 - Bmq + 2aBq\omega, \quad \nu = -\frac{i(BmMq + M\mu_s^2 - 3aBMq\omega - 2M\omega^2)}{k}, \quad (22)$$

the solution regular at spatial infinity can be written schematically as

$$R_{\text{far}} = e^{ix/2} x^l U(1 + l + \epsilon^2 - \nu, 2(1 + l + \epsilon^2), -ix), \quad x = 2kr, \quad (23)$$

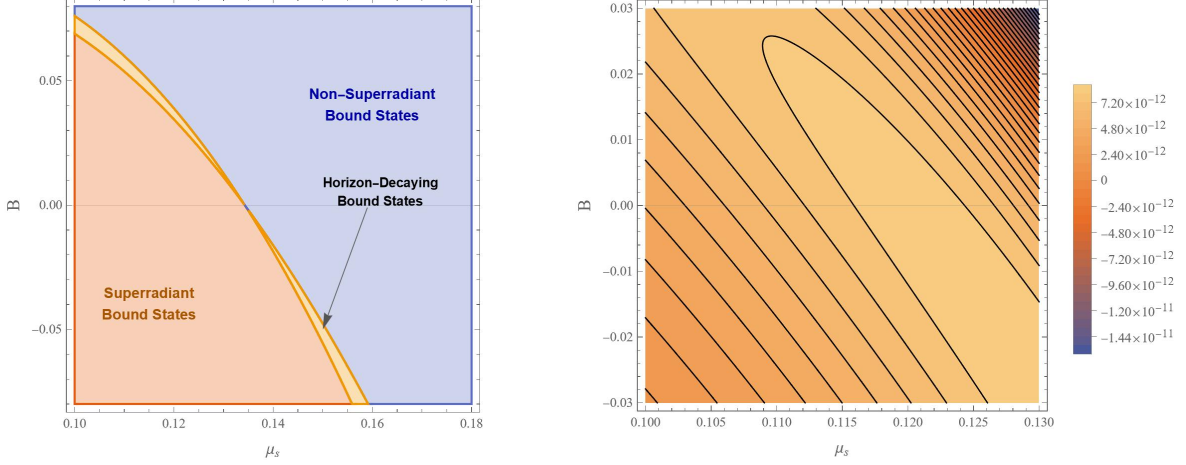


FIG. 1. Left: Parametric phase diagram in the  $(\mu_s, B)$  plane highlighting three distinct bound-state regimes for  $M = 1$ ,  $a = 0.5$ ,  $q = 0.1$ ,  $n = 0$ , and  $l = m = 1$ . The colored regions correspond to Superradiant Bound States (orange), Non-Superradiant Bound States (blue), and the critical Horizon-Decaying Bound States (gold). Right: Contour visualization of the magnitude of instability growth rate  $\gamma = \text{Im}(\delta\omega)$  within the superradiant bound state regime. This panel is directly generated by visualizing the analytical formula, rather than from full numerical integrations, explicitly mapping the continuous transition towards the critical quenching threshold ( $\gamma = 0$ ).

where  $U$  is the confluent hypergeometric function. This solution decays at infinity when  $k = i|k|$ , which is precisely the bound-state condition.

In the near region,  $r - r_+ \ll 1/\sqrt{-k^2}$ , the equation is controlled by the horizon index  $\alpha$ . Introducing  $z = (r - r_+)/ (r_+ - r_-)$ , the physical near-horizon solution takes the form

$$R_{\text{near}} = z^{i\alpha} (1 - z)^{l+1} F(l + 1, l + 1 + 2i\alpha, 1 + 2i\alpha, z), \quad (24)$$

where  $F$  is the Gauss hypergeometric function. For the propagating branch,  $\alpha$  is real and labels the horizon wave phase. For the horizon-decaying branch,  $\alpha^2 < 0$  and the same index is analytically continued to a purely imaginary value, implementing the evanescent boundary condition derived in Sec. III.

Expanding Eqs. (23) and (24) in the overlap region and matching the coefficients of the  $r^l$  and  $r^{-l-1}$  terms gives the resonance condition

$$\frac{\Gamma(-l - \nu - \epsilon^2)\Gamma(2l + 2)}{\Gamma(l - \nu + 1 + \epsilon^2)\Gamma(-2l - 2\epsilon^2)} = -2\alpha [2k(r_+ - r_-)]^{2l+1} \prod_{j=1}^l (j^2 + 4\alpha^2) \frac{\Gamma(l + 1)\Gamma(-2l - 1)}{\Gamma(2l + 1)\Gamma(-l)}. \quad (25)$$

The pole condition in the left-hand side fixes the hydrogenic leading frequency, while the right-hand side gives the small complex correction. More explicitly, the leading quantization condition is

$$l - \nu^{(0)} + 1 + \epsilon^2 = -n, \quad n = 0, 1, 2, \dots, \quad (26)$$

which gives the zero-order real frequency  $\omega^{(0)}$  and the asymptotic wavenumber  $k^{(0)}$ :

$$\omega^{(0)} = \omega_f - \frac{M^2 \left[ \omega_f^2 - \left( a^2 B^2 q^2 - a B q \sqrt{a^2 B^2 q^2 + B m q + \mu_s^2} \right) \right]^2}{2(l+n+1)^2 \sqrt{a^2 B^2 q^2 + B m q + \mu_s^2}}, \quad (27)$$

$$k^{(0)} = i \sqrt{\frac{M^2 \sqrt{a^2 B^2 q^2 + B m q + \mu_s^2} \omega_f^3}{(l+n+1)^2}}. \quad (28)$$

Thus  $k^{(0)}$  is imaginary for the bound state. The perturbative frequency shift  $\delta\omega$  is obtained through

$$\delta\nu = \left. \frac{\partial\nu}{\partial\omega} \right|_{\omega=\omega^{(0)}} \delta\omega, \quad (29)$$

where the variation  $\delta\nu$  is

$$\delta\nu = 2\alpha^{(0)} \left[ 2k^{(0)}(r_+ - r_-) \right]^{2l+1} \frac{(2l+1+n)!}{n!} \left[ \frac{l!}{(2l)!(2l+1)!} \right]^2 \prod_{j=1}^l (j^2 + 4\alpha^{(0)2}). \quad (30)$$

Here,  $\alpha^{(0)} \equiv \alpha(\omega^{(0)})$  is the near-horizon coupling parameter evaluated at the zero-order frequency.

The instability growth rate  $\gamma = \text{Im}(\delta\omega)$  is thus fundamentally dictated by  $\alpha^{(0)}$  and  $k^{(0)}$ .

In conventional superradiant scenarios (the orange regime in Fig. 1),  $\alpha^{(0)}$  is real. Since

$$\left[ k^{(0)} \right]^{2l+1} = i(-1)^l |k^{(0)}|^{2l+1}, \quad (31)$$

Eq. (30) is imaginary at leading order, and hence  $\delta\omega$  has a nonzero imaginary part. The right panel of Fig. 1 displays the magnitude of this growth rate, obtained by directly visualizing the analytical formula in the superradiant bound-state regime.

As explicitly mapped by the contours, the growth rate  $\gamma$  exhibits a coupled dependence on both the scalar mass  $\mu_s$  and the magnetic field strength  $B$ . The parameter space features a distinct “ridge” of maximum instability, representing the optimal balance between superradiant energy extraction and wave confinement. For a fixed magnetic field  $B$ , increasing the scalar mass  $\mu_s$  changes the effective potential well and progressively suppresses the amplification efficiency. Conversely, tuning  $B$  modulates both the asymptotic confinement and the near-horizon electromagnetic coupling. Moving away from the ridge, either by shifting  $\mu_s$  or by adjusting  $B$  toward the critical transition boundary, drives the growth rate down to zero.

When the system crosses this boundary and enters the horizon-decaying regime (the gold band in the left panel of Fig. 1), the parameter  $\alpha^2$  becomes negative. We may write

$$\alpha^{(0)} = i|\alpha^{(0)}|. \quad (32)$$

The extra factor of  $i$  from the horizon index cancels the imaginary phase already carried by the odd power of the bound-state wavenumber:

$$\alpha^{(0)} \left[ k^{(0)} \right]^{2l+1} = i|\alpha^{(0)}| i(-1)^l |k^{(0)}|^{2l+1} = (-1)^{l+1} |\alpha^{(0)}| |k^{(0)}|^{2l+1}. \quad (33)$$

The remaining product  $\prod_{j=1}^l (j^2 + 4\alpha^{(0)2})$  is also real. Therefore  $\delta\nu$ , and hence  $\delta\omega$ , is real at this order:

$$\text{Im}(\delta\omega) = \gamma = 0. \quad (34)$$

This is the analytic quenching mechanism: the same magnetic-rotation coupling that turns the horizon wave into an evanescent mode also removes the leading dissipative imaginary part of the bound-state frequency.

## V. NUMERICAL EVIDENCE FOR THE TWO BRANCHES

To validate the analytical framework and explore the detailed spatial profiles, we solve the Schrödinger-like radial equation (5) numerically via a direct integration method coupled with a shooting algorithm [51]. The detailed numerical strategy is outlined in Appendix D. We focus on the fundamental and overtone modes ( $l = m = 1$ ) with fixed parameters  $M = 1, a = 0.5$ , and  $q = 0.3$  to plot the wavefunctions as  $R(y)$ .

### A. Propagating Reference Clouds (Type-I)

Figure 2 illustrates the radial wavefunctions of the propagating Type-I clouds, which serve as the reference branch for comparison with the horizon-decaying solutions. By tuning the frequency exactly to the lower transition point  $\omega = \omega_1$ , the system sits at the boundary between propagating superradiant modes and the magnetically induced evanescent band. As shown in the left panels, the scalar field decays exponentially at spatial infinity, forming a localized bound state. Notably, the  $\mu_s = 0$  curves confirm that even for a massless scalar field, the external magnetic field provides an effective mass squared ( $\mu_{\text{eff}}^2 = Bmq - 2aBq\omega$ ) at spatial infinity, acting as a potential barrier to support the bound state.

The right panels show that as  $y \rightarrow -\infty$  (approaching the horizon), the amplitude of all wavefunctions plateaus to a non-zero constant. Altering the scalar mass  $\mu_s$  and the magnetic field  $B$  does not change this qualitative near-horizon structure. They all asymptotically approach a constant value, confirming that Type-I clouds are the zero-wavenumber edge of the propagating branch rather than the new evanescent branch.

To further investigate the excitation spectrum, we compare the fundamental mode ( $n = 0$ ) with the overtones ( $n = 1, 2$ ). The overtone number  $n$  corresponds to the number of radial nodes in the

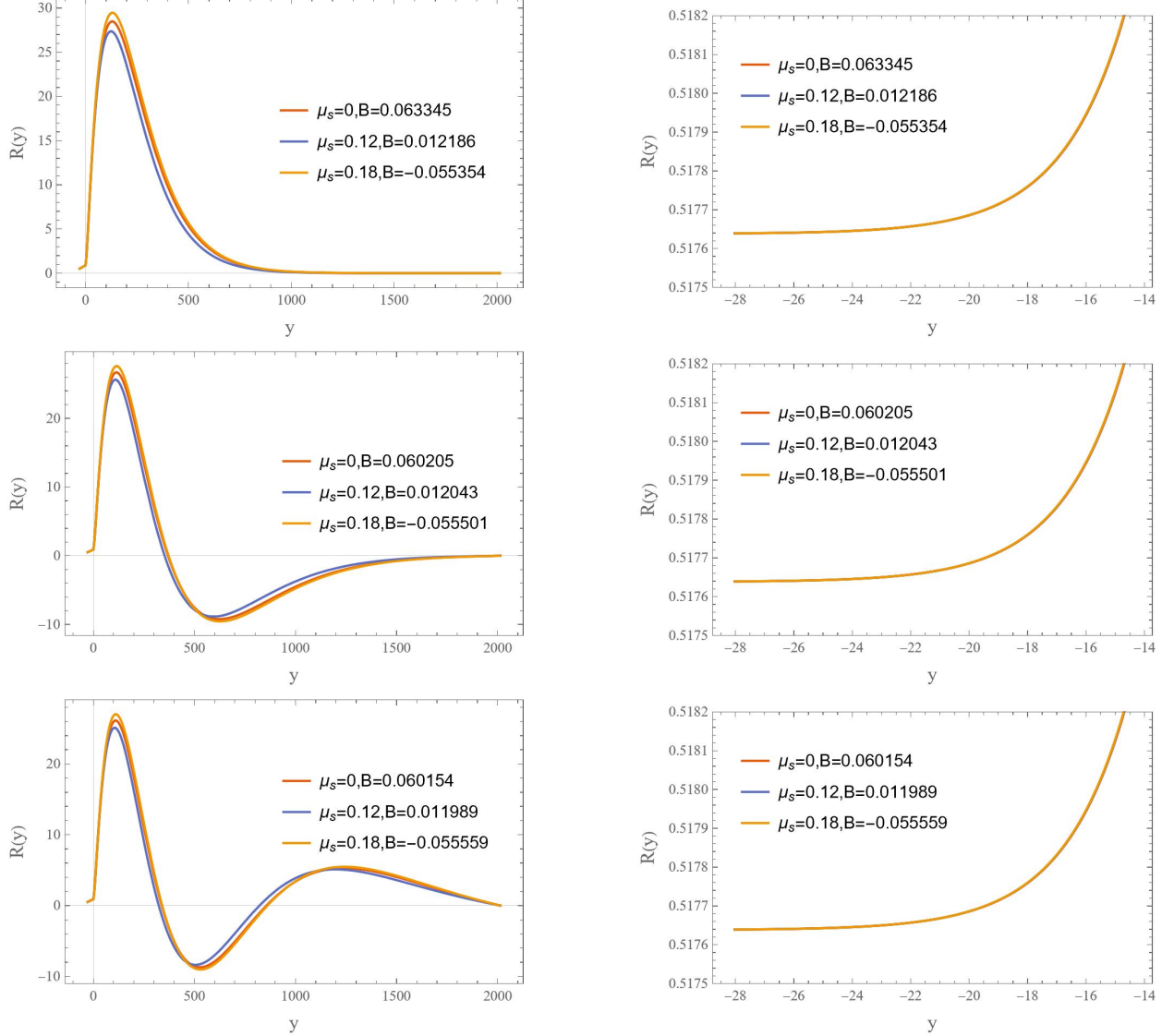


FIG. 2. Radial wavefunctions  $R(y)$  of the propagating Type-I reference clouds ( $n = 0, 1, 2$ ) evaluated at  $\omega = \omega_1$ . Left panels: Global bound-state decay at spatial infinity. Right panels: Near-horizon behavior showing a non-zero constant amplitude, characteristic of the zero-wavenumber edge of the propagating branch.

wavefunction. As shown in Fig. 3, accommodating higher overtones requires precise adjustments to the potential well. The left panel shows that when the scalar mass  $\mu_s$  is fixed, gradually decreasing the magnetic field  $B$  relaxes the spatial confinement, allowing the wavefunction to extend further and excite more radial nodes. Conversely, the right panel demonstrates that when  $B$  is fixed, slightly decreasing  $\mu_s$  achieves a similar spatial extension and overtone excitation.

Figure 4 maps the permissible parameter space and the corresponding critical frequency  $\omega_1$  for these Type-I propagating reference clouds. The upper panels display the  $(\mu_s, B)$  space slices. The

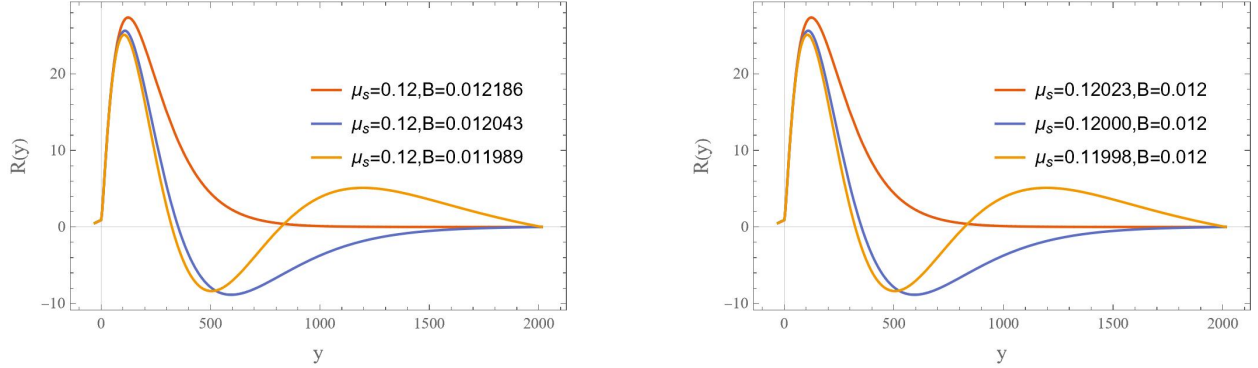


FIG. 3. Comparison of different overtone numbers ( $n = 0, 1, 2$ ) for Type-I propagating reference clouds. Left: Fixed scalar mass  $\mu_s \approx 0.12$ . Right: Fixed magnetic field  $B = 0.012$ . The counterpart parameter must be finely tuned to maintain the synchronized bound state and excite higher nodes.

left panel shows the required  $B$  values for different modes ( $n = 0, 1, 2$ ) at fixed  $\mu_s$ , while the right panel shows the corresponding  $\mu_s$  values at fixed  $B$ . The embedded insets highlight the discrete fine-structure splitting between different overtones. Furthermore, these panels reveal that to satisfy the physical condition  $\mu_s > 0$ , the magnetic field is strictly bounded by  $B < 0.063345$ . The lower panels illustrate how the synchronized frequency  $\omega_1$  evolves with  $B$  (left) and  $\mu_s$  (right), again demonstrating the discrete frequency splitting for different radial nodes in the insets.

### B. Horizon-Decaying Scalar Clouds from Rotation–Magnetic Coupling (Type-II)

Figure 5 depicts the Type-II horizon-decaying scalar clouds evaluated at  $\omega = \omega_c$ , which lies inside the rotation–magnetic quenching band. These solutions are the main new configurations of this work. Similar to Type-I clouds, the  $\mu_s = 0$  curves verify that the effective scalar mass provided by the external magnetic field is sufficient to support these bound states at infinity.

The right panels reveal the key physical difference near the event horizon. Unlike the constant plateau of Type-I clouds, the amplitude of Type-II wavefunctions exponentially decays toward zero as  $y \rightarrow -\infty$ , confirming the  $Y \sim e^{\kappa_h y}$  boundary condition. This behavior is not obtained by merely tuning to a synchronization point; it is produced when the magnetic coupling and black-hole rotation jointly drive  $k_h^2$  negative. Because the magnitude of the decay constant  $\kappa_h$  is small in the examples shown, this exponential decay is strongly stretched and appears visually as a gradual linear growth extending outward from the horizon. Changing  $\mu_s$  and  $B$  directly alters  $\kappa_h$ , resulting in different degrees of exponential decay at the horizon.

The overtone modes ( $n = 1, 2$ ) for Type-II clouds are shown in Fig. 6. Similar to the Type-I

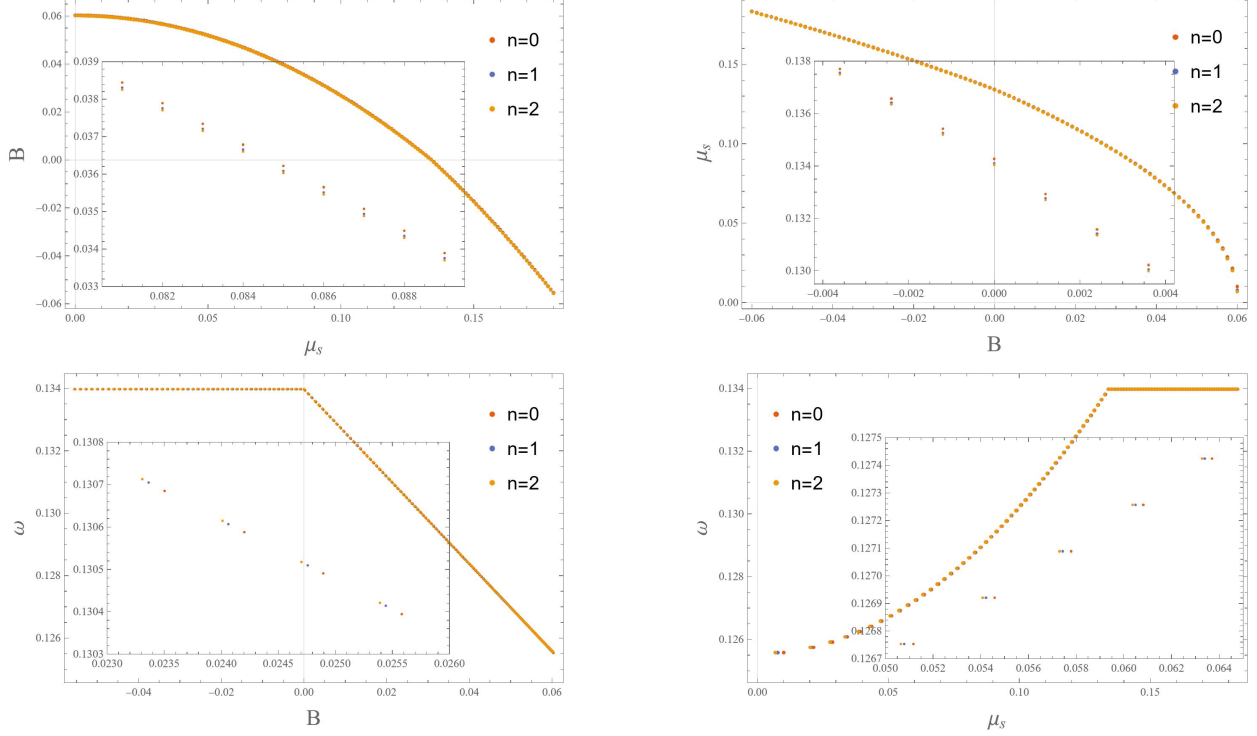


FIG. 4. The permissible parameter space for propagating Type-I reference clouds at  $\omega = \omega_1$ . The upper panels show the bounds on  $\mu_s$  and  $B$ , while the lower panels display the evolution of  $\omega_1$ . The embedded insets resolve the discrete fine-structure splitting induced by the overtone number  $n$ .

branch, supporting higher radial nodes demands a delicate re-balancing of the potential well. The left panel shows that for a fixed  $\mu_s$ , slightly reducing the magnetic field  $B$  allows the field to form additional nodes. The right panel demonstrates that fixing  $B$  and slightly reducing  $\mu_s$  achieves the same effect. This indicates the precise balance between the mass term and the magnetic confinement required to host higher-order horizon-decaying clouds.

Finally, Figure 7 presents the parameter space and critical frequency evolution for Type-II clouds at  $\omega = \omega_c$ . The upper left panel displays the required  $B$  values for different nodes when varying  $\mu_s$ , while the upper right panel shows the corresponding  $\mu_s$  limits when varying  $B$ . A key physical constraint is observed here: to ensure  $\mu_s > 0$  for these specific modes at  $\omega = \omega_c$ , the external magnetic field must be restricted to  $B < 0.064482$ . The lower panels show the evolution of  $\omega_c$  with respect to  $B$  (left) and  $\mu_s$  (right). The insets resolve the discrete fine-structure splitting between different modes, confirming that the horizon-decaying branch is quantized in the same bound-state sense as ordinary scalar clouds while obeying a different horizon boundary condition.

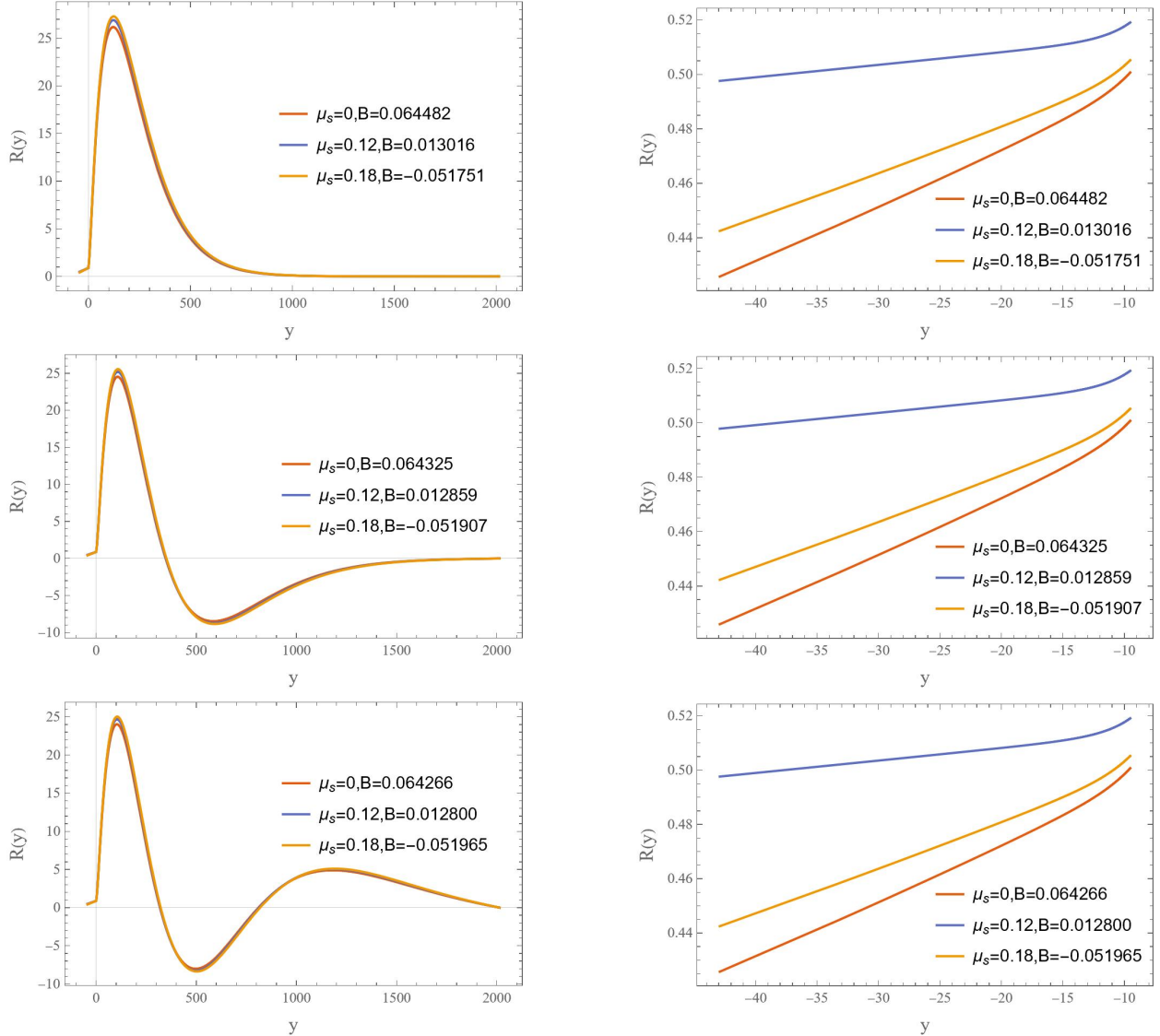


FIG. 5. Radial wavefunctions  $R(y)$  of the horizon-decaying scalar clouds ( $n = 0, 1, 2$ ) at  $\omega = \omega_c$ . The right panels illustrate the exponential decay condition at the event horizon and show that varying parameters directly affect the steepness of the decay.

## VI. DISCUSSION AND OUTLOOK

In this work, we have identified a mechanism by which black-hole rotation and an external magnetic field jointly generate horizon-decaying scalar clouds. The central criterion is the appearance of a positive horizon gap in the near-horizon radial dispersion relation. The Kerr-Bertotti-Robinson geometry was used as a controlled separable setting in which this criterion can be realized and isolated analytically. By deriving the near-horizon boundary conditions and employing matched asymptotic expansions, we showed that the magnetic coupling modifies the rotational superradiant

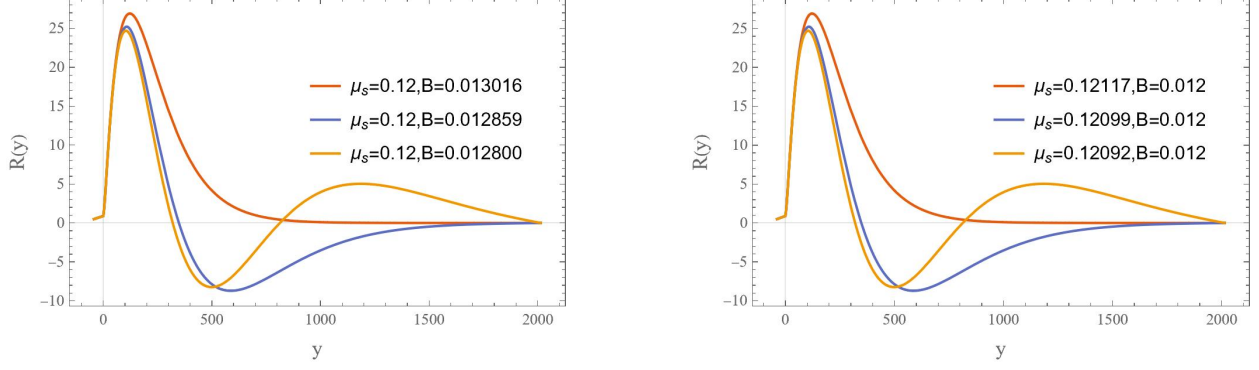


FIG. 6. Comparison of different overtone modes ( $n = 0, 1, 2$ ) for the horizon-decaying scalar clouds at  $\omega = \omega_c$ . Left: Fixed scalar mass  $\mu_s \approx 0.12$ . Right: Fixed magnetic field  $B = 0.012$ .

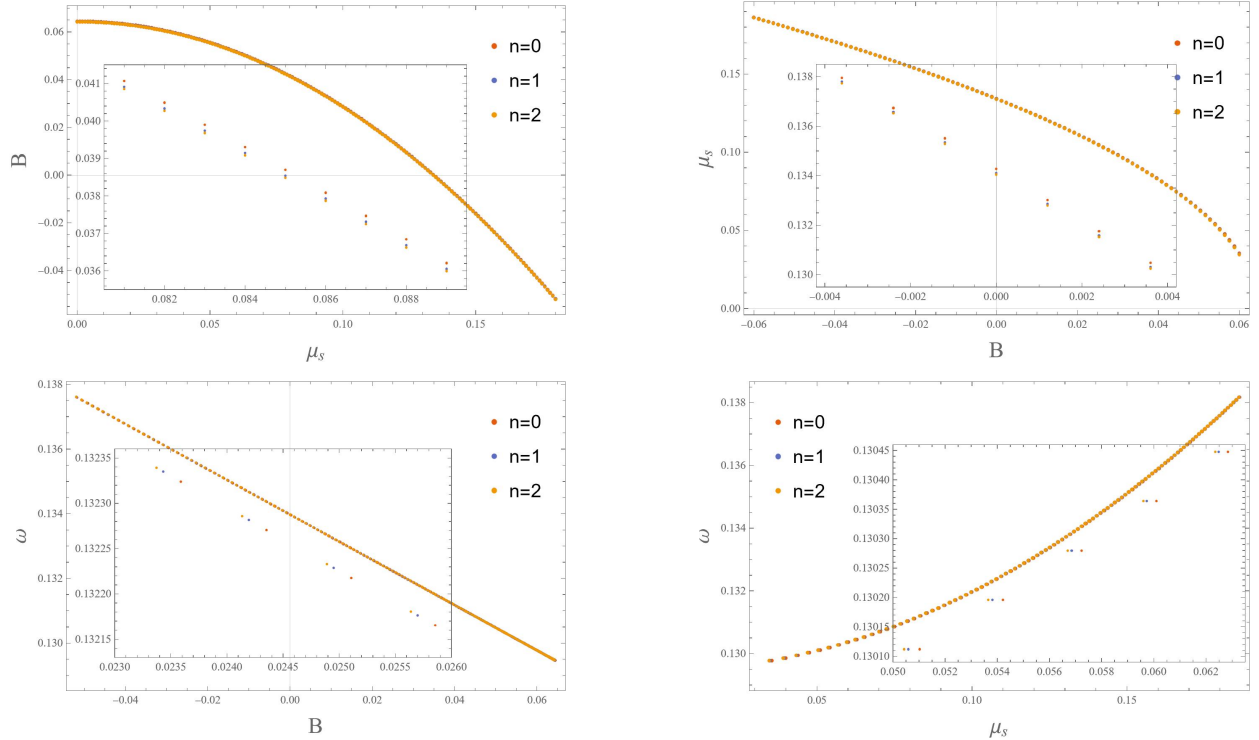


FIG. 7. The permissible parameter space for Type-II horizon-decaying scalar clouds evaluated at  $\omega = \omega_c$ . The upper panels show the parameter bounds, and the lower panels show the frequency evolution. The insets resolve the discrete fine-structure splitting required to support higher nodal numbers.

channel and creates a finite evanescent band in the bound-state spectrum.

Specifically, the fundamental manifestation of this rotation–magnetic quenching is that the propagating superradiant branch terminates *before* the scalar field frequency reaches the kinematic synchronization threshold  $\omega_c$ . This premature termination creates a transition band ( $\omega_1 < \omega < \omega_2$ ) in which the horizon wavenumber is imaginary. Consequently, the system supports two stationary

configurations with different horizon physics:

**Type-I: Propagating reference clouds**

These clouds lie on the lower boundary of the quenching transition band ( $\omega = \omega_1$ ). They are the zero-wavenumber edge of the propagating branch. Their near-horizon amplitude approaches a non-zero plateau, providing a useful reference against which the new horizon-decaying solutions can be distinguished.

**Type-II: Horizon-decaying scalar clouds**

Inside the transition band ( $\omega_1 < \omega < \omega_2$ ), the effective wavenumber at the horizon becomes purely imaginary ( $k_h^2 < 0$ ). The scalar field therefore obeys an evanescent boundary condition and decays exponentially toward the horizon. This is the principal new branch found in this work. Its existence is tied to the simultaneous presence of rotation and magnetic coupling: rotation provides the superradiant channel, while the magnetic field reshapes the near-horizon dispersion relation so that the channel is converted into a zero-flux evanescent state. In the language of the general criterion, the Kerr-BR calculation supplies an explicit positive-gap realization, rather than merely an additional example of synchronized clouds. The small decay constant  $\kappa_h$  gives these clouds a characteristic near-horizon profile that appears as a gradual outward growth in the numerical solutions.

The positive-gap criterion proposed here should be understood as a conditional near-horizon statement. It applies when the charged scalar equation can be separated, or reduced near the horizon after a regular field redefinition, to a radial equation of the form in Eq. (16). Establishing whether the same gap appears in fully nonseparable magnetized Kerr geometries, including higher-order magnetic backreaction and angular mode mixing, remains an open problem.

Our current analytical and numerical frameworks are based on the linear test-field approximation in the frequency domain. A natural next step is to test the time-domain evolution and non-linear stability of the Type-II branch. In particular, it would be important to determine whether the horizon-evanescent boundary condition remains robust under dynamical perturbations and backreaction. Furthermore, our analytical mapping relies on the weak magnetic field approximation ( $B \ll 1/M$ ). In geometrized units, the characteristic magnetic field  $B_M \sim 1/M$  corresponds to an extreme field strength of  $\mathcal{O}(10^{19} M_\odot/M)$  Gauss [53–55]. While the weak-field limit covers a broad range of astrophysically motivated scenarios, exploring the deformation of the Type-II branch in ultra-strong magnetic fields (e.g.,  $B \sim 0.1/M$ ), where the  $\mathcal{O}(B^2)$  spacetime backreaction and higher-order angular couplings cannot be perturbatively decoupled, remains an open theoretical challenge. Investigating whether these horizon-decaying clouds can seed non-linear hair

or generate observational signatures would clarify the broader relevance of the rotation–magnetic-field mechanism.

### Appendix A: Technical Details: Field Equations

Under the assumption  $B \ll 1$  and explicitly setting the electromagnetic phase parameter  $\xi = 0$ , separating the variables  $\Phi = \sum_{l,m} e^{i(m\phi - \omega t)} R(r) S(\theta)$  yields the following unapproximated, fully coupled ordinary differential equations.

The radial equation is given by:

$$\begin{aligned}
& \frac{1}{R(r)} \frac{d}{dr} [(a^2 - 2Mr + r^2)R'(r)] \\
& + \frac{1}{2}\mu_s^2 \left( \frac{a^4}{a^2 + r(-2M + r)} + \frac{a^2(2M - 3r)r}{a^2 + r(-2M + r)} + \frac{2(2M - r)r^3}{a^2 + r(-2M + r)} + a^2 \right) \\
& + \frac{1}{2}\omega^2 \left( \frac{a^4}{a^2 + r(-2M + r)} + \frac{2r^4}{a^2 + r(-2M + r)} + \frac{a^2r(2M + 3r)}{a^2 + r(-2M + r)} - a^2 \right) \\
& + \omega \left( \frac{4amMr}{a^2 + r(-2M + r)} + \frac{1}{2} \left( \frac{2a^5Bq}{a^2 + r(-2M + r)} + \frac{4aBqr^3(-M + r)}{a^2 + r(-2M + r)} \right. \right. \\
& \left. \left. + \frac{2a^3Bqr(-2M + 3r)}{a^2 + r(-2M + r)} - 2a^3Bq \right) \right) \\
& + \frac{1}{2}m^2 \frac{2a^2}{a^2 + r(-2M + r)} + \frac{1}{2}m \left( \frac{a^4Bq}{a^2 + r(-2M + r)} + \frac{2Bq(2M - r)r^3}{a^2 + r(-2M + r)} \right. \\
& \left. - \frac{a^2Bqr(2M + 3r)}{a^2 + r(-2M + r)} + a^2Bq \right) - K = 0.
\end{aligned} \tag{A1}$$

The corresponding angular equation takes the form of a generalized prolate spheroidal wave equation:

$$\begin{aligned}
& \frac{1}{S(\theta) \sin \theta} \frac{d}{d\theta} (\sin \theta S'(\theta)) - \frac{1}{2}\mu_s^2 a^2 \cdot 2 \cos^2 \theta + \frac{1}{2}\omega^2 a^2 \cdot 2 \cos^2 \theta \\
& + \frac{1}{2}\omega \cdot 2a^3Bq \cdot 2 \cos^2 \theta - \frac{1}{2}m^2 \cdot 2 \csc^2 \theta - \frac{1}{2}ma^2Bq \cdot 2 \cos^2 \theta - \frac{1}{2}m \cdot 2a^2Bq \csc^2 \theta + K = 0.
\end{aligned} \tag{A2}$$

By introducing the substitution  $x = \cos \theta$ , the angular equation can be recast into the standard form of a generalized prolate spheroidal wave equation. In the limit where the effective spheroidicity parameter  $c^2$  vanishes, the equation reduces to the standard associated Legendre differential equation, and its solutions become the associated Legendre polynomials  $P_l^m(x)$ .

For small but non-zero values of  $c^2$ , which is strictly valid under the weak magnetic field approximation ( $B \ll 1$ ), the spheroidal term  $c^2x^2$  can be treated as a perturbation to the Legendre equation. In this regime, using standard perturbation theory [12, 49], the generalized eigenvalue

separation constant  $K$  can be approximated to first order in  $c^2$  as:

$$K \simeq l(l+1) + \frac{2c^2 \left(m^2 + \frac{1}{2} - l(l+1)\right)}{(2l+3)(2l-1)} + a(2m\omega + a(\mu_s^2 - \omega^2)), \quad (\text{A3})$$

$$c^2 = a^2 Bmq + a^2 \mu_s^2 - 2a^3 Bq\omega - a^2 \omega^2.$$

Furthermore, to analyze the physical boundary conditions and the properties of the bound states, it is useful to map the radial equation into a one-dimensional Schrödinger-like form. By redefining the radial wave function as  $Y(r) = \sqrt{r^2 + a^2} R(r)$ , the radial equation can be recast as:

$$\frac{a^2 - 2Mr + r^2}{r^2 + a^2} \cdot \frac{d}{dr} \left[ \frac{a^2 - 2Mr + r^2}{r^2 + a^2} \cdot \frac{dY(r)}{dr} \right] - V_{\text{eff}}(r) \cdot Y(r) = 0, \quad (\text{A4})$$

where  $V_{\text{eff}}(r)$  is the exact effective potential governing the macroscopic dynamics of the massive scalar field. Collecting all the coupled terms, its full unapproximated expression is explicitly given by:

$$V_{\text{eff}}(r) = - \left\{ - \frac{r(-2M+2r)(a^2-2Mr+r^2)}{(a^2+r^2)^{3/2}} + \frac{3r^2(a^2-2Mr+r^2)^2}{(a^2+r^2)^{5/2}} - \frac{(a^2-2Mr+r^2)^2}{(a^2+r^2)^{3/2}} \right. \\ + \frac{a^2-2Mr+r^2}{\sqrt{a^2+r^2}} \left[ -K + \frac{a^2 m^2}{a^2+r(-2M+r)} \right. \\ + \frac{m}{2} \left( a^2 Bq + \frac{a^4 Bq}{a^2+r(-2M+r)} + \frac{2Bq(2M-r)r^3}{a^2+r(-2M+r)} - \frac{a^2 Bqr(2M+3r)}{a^2+r(-2M+r)} \right) \\ + \frac{\mu_s^2}{2} \left( a^2 - \frac{a^4}{a^2+r(-2M+r)} + \frac{a^2(2M-3r)r}{a^2+r(-2M+r)} + \frac{2(2M-r)r^3}{a^2+r(-2M+r)} \right) \\ + \omega \left( -\frac{4amMr}{a^2+r(-2M+r)} + \frac{1}{2} \left( -2a^3 Bq + \frac{2a^5 Bq}{a^2+r(-2M+r)} \right. \right. \\ \left. \left. + \frac{4aBqr^3(-M+r)}{a^2+r(-2M+r)} + \frac{2a^3 Bqr(-2M+3r)}{a^2+r(-2M+r)} \right) \right) \\ \left. \left. + \frac{\omega^2}{2} \left( -a^2 + \frac{a^4}{a^2+r(-2M+r)} + \frac{2r^4}{a^2+r(-2M+r)} + \frac{a^2 r(2M+3r)}{a^2+r(-2M+r)} \right) \right] \right\} \\ \times \frac{1}{(a^2+r^2)^{3/2}}. \quad (\text{A5})$$

## Appendix B: Technical Details: Bound-State Constraints

The physical horizon boundary condition is discussed in Sec. III. Here we collect the remaining bound-state constraints at spatial infinity, which determine when the radial solution is localized rather than radiative.

To ensure the scalar field forms a bound state rather than radiating to infinity,  $k_f^2 > 0$  must be strictly maintained. This imposes the following parameter space constraints on the scalar mass  $\mu_s$  and azimuthal number  $m \in \mathbb{Z}$ :

If  $-1 < q < 0$ :

$$\left\{ \begin{array}{l} -1 < B < 0 \text{ and } a > 0 \text{ and } \begin{cases} m \leq 0 \text{ and } M > a \text{ and } \mu_s > \sqrt{-Bmq} \\ m \geq 1 \text{ and } M > a \text{ and } \mu_s \geq 0 \end{cases} \\ B = 0 \text{ and } a > 0 \text{ and } M > a \text{ and } \mu_s > 0 \\ 0 < B < 1 \text{ and } a > 0 \text{ and } \begin{cases} m \leq -a^2Bq \text{ and } M > a \text{ and } \mu_s \geq 0 \\ m > -a^2Bq \text{ and } M > a \text{ and } \mu_s \geq \sqrt{-a^2B^2q^2 - Bmq} \end{cases} \end{array} \right. \quad (\text{B1})$$

If  $q = 0$ :

$$-1 < B < 1 \text{ and } a > 0 \text{ and } M > a \text{ and } \mu_s > 0 \quad (\text{B2})$$

If  $0 < q < 1$ :

$$\left\{ \begin{array}{l} -1 < B < 0 \text{ and } a > 0 \text{ and } \begin{cases} m \leq -a^2Bq \text{ and } M > a \text{ and } \mu_s \geq 0 \\ m > -a^2Bq \text{ and } M > a \text{ and } \mu_s \geq \sqrt{-a^2B^2q^2 - Bmq} \end{cases} \\ B = 0 \text{ and } a > 0 \text{ and } M > a \text{ and } \mu_s > 0 \\ 0 < B < 1 \text{ and } a > 0 \text{ and } \begin{cases} m \leq 0 \text{ and } M > a \text{ and } \mu_s > \sqrt{-Bmq} \\ m \geq 1 \text{ and } M > a \text{ and } \mu_s \geq 0 \end{cases} \end{array} \right. \quad (\text{B3})$$

### Appendix C: Technical Details: Matched Asymptotic Expansion

Following the analytical framework originally established by Detweiler [13] and extensively utilized by Furuhashi and Nambu for massive scalar fields [14], we perform a matched asymptotic expansion to analytically map the complex frequency  $\omega$ .

For values of  $r \gg M$ , the radial equation is approximately:

$$\frac{d^2}{dr^2} (rR) + \left[ k^2 - \frac{2i\nu k}{r} - \frac{l(l+1) + \epsilon^2}{r^2} \right] rR = 0, \quad (\text{C1})$$

with definitions  $k \equiv \sqrt{-Bmq - \mu_s^2 + 2aBq\omega + \omega^2}$ ,  $\nu \equiv -i(BmMq + M\mu_s^2 - 3aBMq\omega - 2M\omega^2)/k$ , and  $x = 2kr$ . The solution regular at infinity is  $R(x) = e^{ix/2} x^l {}_2U(1+l+\epsilon^2-\nu, 2(1+l+\epsilon^2), -ix)$ , where  ${}_2U$  is the confluent hypergeometric function of the second kind [49]. Its asymptotic behavior for  $|kr| \ll 1$  is:

$$R \sim \frac{2^l (kr)^l \Gamma(-1-2l-2\epsilon^2)}{\Gamma(-l-\epsilon^2-\nu)} - \frac{2^{-1-l} (kr)^{-1-l} \Gamma(1+2l+2\epsilon^2)}{e^{2il\pi} \Gamma(1+l+\epsilon^2-\nu)}. \quad (\text{C2})$$

Conversely, when  $r \ll l/\mu_s$ , transforming to  $z = (r - r_+)/ (r_+ - r_-)$  simplifies the equation to:

$$z(z+1) \frac{d}{dz} \left[ z(z+1) \frac{dR}{dz} \right] + [\alpha^2 - l(l+1)z(z+1)]R = 0, \quad (\text{C3})$$

where the near-horizon coupling parameter  $\alpha^2$  is explicitly given by:

$$\alpha^2 \equiv \frac{1}{4(a^2 - M^2)} \left[ -a^4 Bmq + a^3 BMq\omega(6M - r_- + r_+) \right. \\ \left. + a^2(2BmMqr_+ - m^2 + 4M^2\omega^2) + 4aMr_+\omega(m - 2BM^2q) - 8M^3r_+\omega^2 \right]. \quad (\text{C4})$$

When  $B \ll 1$  and outside the quenching band ( $\omega < \omega_1$  or  $\omega > \omega_2$ ),  $\alpha$  is real and can be approximated as  $\alpha \simeq \alpha_0 + \frac{\alpha_B^2}{2\alpha_0}$ , where

$$\alpha_0 = \frac{am - 2Mr_+\omega}{r_+ - r_-}, \quad \alpha_B = \frac{1}{2} \sqrt{-\frac{aBq(a^3m + a^2M\omega(-6M + r_- - r_+) - 2amMr_+ + 8M^3r_+\omega)}{a^2 - M^2}}. \quad (\text{C5})$$

The general solution at the horizon ( $z \rightarrow 0$ ) is:

$$R(z) = z^{i\alpha}(1-z)^{l+1} F(l+1, l+1+2i\alpha, 1+2i\alpha, z). \quad (\text{C6})$$

where  $F$  is the Gauss hypergeometric function [49]. Evaluating its asymptotic form for  $z \gg 0$ :

$$R \sim \frac{\Gamma(1+2i\alpha)\Gamma(2l+1)}{\Gamma(l+1)\Gamma(l+1+2i\alpha)} \left( \frac{r}{r_+ - r_-} \right)^l + \frac{\Gamma(1+2i\alpha)\Gamma(-2l-1)}{\Gamma(-l)\Gamma(-l+2i\alpha)} \left( \frac{r}{r_+ - r_-} \right)^{-l-1}. \quad (\text{C7})$$

In the overlap region  $r_+ \ll r \ll 1/\sqrt{-k^2}$ , matching the leading-order terms of Eq. (C2) and (C7) yields the resonance condition [13, 14]:

$$\frac{\Gamma(-l-\nu-\epsilon^2)\Gamma(2l+2)}{\Gamma(l-\nu+1+\epsilon^2)\Gamma(-2l-2\epsilon^2)} = -2\alpha [2k(r_+ - r_-)]^{2l+1} \prod_{j=1}^l (j^2 + 4\alpha^2) \frac{\Gamma(l+1)\Gamma(-2l-1)}{\Gamma(2l+1)\Gamma(-l)}. \quad (\text{C8})$$

Defining  $\nu^{(0)}$  such that  $l - \nu^{(0)} + 1 + \epsilon^2 = -n$ , we substitute  $\nu \equiv \nu^{(0)} + \delta\nu$  to isolate the perturbative shift:

$$\nu^{(0)} = -\frac{i \left( BmMq + M\mu_s^2 - 3aBMq\omega^{(0)} - 2M\omega^{(0)2} \right)}{\sqrt{-Bmq - \mu_s^2 + 2aBq\omega^{(0)} + \omega^{(0)2}}} \simeq l + n + 1 \quad (\text{C9})$$

$$\omega^{(0)} = \omega_f - \frac{M^2(\omega_f^2 - (a^2B^2q^2 - aBq\sqrt{a^2B^2q^2 + Bmq + \mu_s^2}))^2}{2(l+n+1)^2 \sqrt{a^2B^2q^2 + Bmq + \mu_s^2}}, \quad (\text{C10})$$

$$k^{(0)} = i \sqrt{\frac{M^2 \sqrt{a^2B^2q^2 + Bmq + \mu_s^2} \omega_f^3}{(l+n+1)^2}}, \quad (\text{C11})$$

$$\delta\nu = 2\alpha^{(0)} \left[ 2k^{(0)}(r_+ - r_-) \right]^{2l+1} \frac{(2l+1+n)!}{n!} \left[ \frac{l!}{(2l)!(2l+1)!} \right]^2 \prod_{j=1}^l (j^2 + 4\alpha^{(0)2}). \quad (\text{C12})$$

The relation between the frequency shift and  $\delta\nu$  is  $\delta\nu = \left. \frac{\partial\nu}{\partial\omega} \right|_{(\omega=\omega^{(0)})} \delta\omega$ . Therefore, the real part  $\sigma = \omega^{(0)}$  and the imaginary part  $\gamma = \text{Im}(\delta\omega)$  are the leading-order contribution to the eigenvalue  $\omega$ , which is fundamentally consistent with the unstable mode analysis developed by Damour *et al.* [11].

The crucial step occurs when investigating the exponentially decaying regime where  $\alpha^2 < 0$ . The parameter  $\alpha^{(0)}$  undergoes an analytic continuation into a purely imaginary value:  $\alpha^{(0)} = \alpha_1^{(0)} \simeq i \left( \alpha_0 + \frac{\alpha_B^2}{2\alpha_0} \right)$ .

Notice that the zero-order asymptotic wavenumber  $k^{(0)}$  is strictly imaginary,  $k^{(0)} = i|k^{(0)}|$ . Consequently, the factor involving  $k^{(0)}$  yields an imaginary phase:  $[k^{(0)}]^{2l+1} = i^{2l+1}|k^{(0)}|^{2l+1} = i(-1)^l|k^{(0)}|^{2l+1}$ .

When the system enters the exponentially decaying regime, the linear factor  $\alpha^{(0)}$  contributes an additional factor of  $i$ . The product of these two imaginary phases yields:

$$\alpha_1^{(0)} \cdot [k^{(0)}]^{2l+1} \propto (i|\alpha_1^{(0)}|) \cdot (i(-1)^l|k^{(0)}|^{2l+1}) = (-1)^{l+1}|\alpha_1^{(0)}||k^{(0)}|^{2l+1}. \quad (\text{C13})$$

Because  $i \times i = -1$ , the imaginary units exactly cancel out. Since the product term  $\prod_{j=1}^l (j^2 + 4\alpha^{(0)2}) = \prod_{j=1}^l (j^2 - 4|\alpha_1^{(0)}|^2)$  remains strictly real, and the background derivative  $\left. \frac{\partial\nu}{\partial\omega} \right|_{(\omega=\omega^{(0)})}$  is also a real quantity, the frequency shift  $\delta\omega$  is forced to be purely real. Therefore,  $\gamma = \text{Im}(\delta\omega) = 0$ .

#### Appendix D: Technical Details: Numerical Calculation Strategy

To numerically integrate the radial equation (5), the radial function  $Y(r)$  is expanded in a Frobenius series near the event horizon to obtain the initial conditions:

$$Y(r) = (r - r_+)^{\sigma} \sum_{j=0}^N Y_j (r - r_+)^j, \quad r \rightarrow r_+, \quad (\text{D1})$$

where the characteristic exponent is  $\sigma = i\sqrt{4(M^2 - a^2)\alpha^2/\Delta'_0(r_+)}$ . By inserting this expansion into the radial equation, the higher-order coefficients  $Y_j$  ( $j \geq 1$ ) can be solved recursively in terms of  $Y_0$ . Since the differential equation is linear, we fix  $Y_0 = 1$  without loss of generality.

In practical numerical calculations, we truncate the infinite radial domain to  $r \in [r_{+n}, r_{\text{INF}}]$ , where  $r_{+n} = r_+(1 + \epsilon)$  is a point very close to the horizon with a small parameter  $\epsilon$ , and  $r_{\text{INF}}$  is a sufficiently large cutoff. We use the near-horizon expansion evaluated at  $r_{+n}$  to provide the initial

values  $Y(r_{+n})$  and  $Y'(r_{+n})$ . From this inner boundary, we perform a *direct numerical integration* outward to  $r_{\text{INF}}$ .

The two kinds of scalar clouds are determined by a set of five parameters  $\{a, q, \omega, \mu_s, B\}$ . When the black hole spin  $a$ , scalar charge  $q$ , and field frequency  $\omega$  are fixed, only specific discrete values of the remaining parameters  $\{\mu_s, B\}$  allow for a bounded solution where  $Y(r \rightarrow \infty) = 0$  to be achieved. Specifically, for fixed  $\{a, q, \omega\}$ , there exist two infinite countable sets of coupling constants,  $\{\mu_s(a, q, \omega, B; n)\}_{n=0}^{\infty}$  and  $\{B(a, q, \omega, \mu_s; n)\}_{n=0}^{\infty}$ , which can support the bounded scalar clouds. The integer  $n$  labels the number of radial nodes of the solution.

By employing a shooting method [51] over these parameter spaces, we iteratively adjust the tuning parameter (either  $\mu_s$  or  $B$ ) until the integrated wavefunction satisfies the asymptotic bound-state boundary condition, exponentially decaying to zero at the outer boundary ( $Y(r_{\text{INF}}) \rightarrow 0$ ). For our computations, we typically set  $N = 3$ ,  $\epsilon = 10^{-9}$ , and  $r_{\text{INF}} = 1500r_+$ .

## ACKNOWLEDGMENTS

This work is supported by the National Natural Science Foundation of China (NNSFC) under Grant No 12075207.

- 
- [1] R. Penrose, “Gravitational collapse: The role of general relativity,” *Riv. Nuovo Cim.* **1** (1969) 252–276.
  - [2] D. Christodoulou, “Reversible and irreversible transformations in black-hole physics,” *Physical Review Letters* **25** no. 25, (1970) 1596.
  - [3] R. Ruffini and J. A. Wheeler, “Introducing the black hole,” *Physics Today* **24** no. 1, (1971) 30–41.
  - [4] Y. B. Zeldovich, “Generation of Waves by a Rotating Body,” *Soviet Journal of Experimental and Theoretical Physics Letters* **14** (1971) 180.
  - [5] Y. B. Zeldovich, “Amplification of Cylindrical Electromagnetic Waves Reflected from a Rotating Body,” *Soviet Journal of Experimental and Theoretical Physics* **35** (1972) 1085.
  - [6] C. W. Misner, “Interpretation of gravitational-wave observations,” *Physical Review Letters* **28** no. 15, (1972) 994.
  - [7] A. A. Starobinskii, “Amplification of waves during reflection from a rotating ”black hole”,” *Sov. Phys. JETP* **37** no. 1, (1973) 28–32.
  - [8] J. D. Bekenstein, “Extraction of energy and charge from a black hole,” *Physical Review D* **7** no. 4, (1973) 949.

- [9] S. A. Teukolsky, “Perturbations of a rotating black hole. i. fundamental equations for gravitational, electromagnetic, and neutrino-field perturbations,” *The Astrophysical Journal* **185** (1973) 635–648.
- [10] W. H. Press and S. A. Teukolsky, “Floating orbits, superradiant scattering and the black-hole bomb,” *Nature* **238** no. 5361, (1972) 211–212.
- [11] T. Damour, N. Deruelle, and R. Ruffini, “On quantum resonances in stationary geometries,” *Lett. Nuovo Cim.* **15** no. 8, (1976) 257–262.
- [12] T. J. M. Zouros and D. M. Eardley, “Instabilities of massive scalar perturbations of a rotating black hole,” *Annals of Physics* **118** no. 1, (1979) 139–155.
- [13] S. Detweiler, “Klein-gordon equation and rotating black holes,” *Physical Review D* **22** no. 10, (1980) 2323.
- [14] H. Furuhashi and Y. Nambu, “Instability of massive scalar fields in kerr-newman spacetime,” *Progress of Theoretical Physics* **112** no. 6, (2004) 983–995.
- [15] V. Cardoso, O. J. C. Dias, J. P. S. Lemos, and S. Yoshida, “Black-hole bomb and superradiant instabilities,” *Physical Review D* **70** no. 4, (2004) 044039.
- [16] S. R. Dolan, “Instability of the massive klein-gordon field on the kerr spacetime,” *Physical Review D* **76** no. 8, (2007) 084001.
- [17] S. R. Dolan, “Superradiant instabilities of rotating black holes in the time domain,” *Physical Review D* **87** no. 12, (2013) 124026.
- [18] H. Witek, V. Cardoso, A. Ishibashi, and U. Sperhake, “Superradiant instabilities in astrophysical systems,” *Physical Review D* **87** no. 4, (2013) 043513.
- [19] R. Brito, V. Cardoso, and P. Pani, “Superradiance: New Frontiers in Black Hole Physics,” *Lect. Notes Phys.* **906** (2015) pp.1–237, [arXiv:1501.06570](https://arxiv.org/abs/1501.06570) [gr-qc].
- [20] S. Hod, “Stationary scalar clouds around rotating black holes,” *Physical Review D* **86** no. 10, (2012) 104026.
- [21] S. Hod, “Kerr-newman black holes with stationary charged scalar clouds,” *Physical Review D* **90** no. 2, (2014) 024051.
- [22] C. A. R. Herdeiro and E. Radu, “Kerr black holes with scalar hair,” *Physical Review Letters* **112** no. 22, (2014) 221101.
- [23] C. A. R. Herdeiro and E. Radu, “Construction and physical properties of kerr black holes with scalar hair,” *Classical and Quantum Gravity* **32** no. 14, (2015) 144001.
- [24] C. L. Benone, L. C. B. Crispino, C. A. R. Herdeiro, and E. Radu, “Kerr-newman scalar clouds,” *Physical Review D* **90** no. 10, (2014) 104024.
- [25] Y. Huang, D.-J. Liu, X.-H. Zhai, and X.-Z. Li, “Scalar clouds around Kerr–Sen black holes,” *Class. Quant. Grav.* **34** no. 15, (2017) 155002, [arXiv:1706.04441](https://arxiv.org/abs/1706.04441) [gr-qc].
- [26] C. A. R. Herdeiro and E. Radu, “Asymptotically flat black holes with scalar hair: a review,” *Int. J. Mod. Phys. D* **24** no. 09, (2015) 1542014, [arXiv:1504.08209](https://arxiv.org/abs/1504.08209) [gr-qc].
- [27] P. Pani, V. Cardoso, L. Gualtieri, E. Berti, and A. Ishibashi, “Black-hole bomb and photon-mass

- bounds,” *Physical Review Letters* **109** no. 13, (2012) 131102.
- [28] W. E. East and F. Pretorius, “Superradiant instability and backreaction of massive vector fields around kerr black holes,” *Phys. Rev. Lett.* **119** (Jul, 2017) 041101.  
<https://link.aps.org/doi/10.1103/PhysRevLett.119.041101>.
- [29] C. Herdeiro, E. Radu, and H. Rúnarsson, “Kerr black holes with proca hair,” *Classical and Quantum Gravity* **33** no. 15, (2016) 154001.
- [30] S. Hod, “Stationary scalar clouds supported by rapidly-rotating acoustic black holes in a photon-fluid model,” *Physical Review D* **103** no. 8, (2021) 084003.
- [31] M. Ciszak and F. Marino, “Acoustic black-hole bombs and scalar clouds in a photon-fluid model,” *Physical Review D* **103** no. 4, (2021) 045004.
- [32] R. D. Blandford and R. L. Znajek, “Electromagnetic extraction of energy from kerr black holes,” *Monthly Notices of the Royal Astronomical Society* **179** no. 3, (1977) 433–456.
- [33] R. M. Wald, “Black hole in a uniform magnetic field,” *Physical Review D* **10** no. 6, (1974) 1680.
- [34] F. J. Ernst, “Kerr black holes in a magnetic universe,” *Journal of Mathematical Physics* **17** no. 1, (1976) 54–56.
- [35] M. A. Melvin, “Pure magnetic and magic electric geons,” *Physics Letters* **8** no. 1, (1964) 65–68.
- [36] G. W. Gibbons, A. H. Mujtaba, and C. N. Pope, “Ergoregions in magnetised black hole spacetimes,” *Classical and Quantum Gravity* **30** no. 12, (2013) 125008.
- [37] M. Astorino, “Thermodynamics of Regular Accelerating Black Holes,” *Phys. Rev. D* **95** no. 6, (2017) 064007, [arXiv:1612.04387 \[gr-qc\]](https://arxiv.org/abs/1612.04387).
- [38] I. Booth, M. Hunt, A. Palomo-Lozano, and H. K. Kunduri, “Insights from melvin–kerr–newman spacetimes,” *Classical and Quantum Gravity* **32** no. 23, (2015) 235025.
- [39] S. M. Wagh, S. V. Dhurandhar, and N. Dadhich, “Revival of penrose process for astrophysical applications,” *Atrophys. J.* **301** (1986) 1018.
- [40] S. M. Wagh and N. Dadhich, “The energetics of black holes in electromagnetic fields by the penrose process,” *Phys. Rept.* **183** no. 4, (1989) 137–192.
- [41] R. A. Konoplya, “Magnetized black hole as a gravitational lens,” *Phys. Lett. B* **644** (2007) 219–223, [arXiv:gr-qc/0608066](https://arxiv.org/abs/gr-qc/0608066).
- [42] R. A. Konoplya, “Magnetic field creates strong superradiant instability,” *Phys. Lett. B* **666** (2008) 283–287, [arXiv:0801.0846 \[hep-th\]](https://arxiv.org/abs/0801.0846).
- [43] R. Brito, V. Cardoso, and P. Pani, “Superradiant instability of black holes immersed in a magnetic field,” *Physical Review D* **89** no. 10, (2014) 104045.
- [44] N. M. Santos and C. A. R. Herdeiro, “Black holes, stationary clouds and magnetic fields,” *Physics Letters B* **815** (2021) 136142.
- [45] J. Podolský and H. Ovcharenko, “Kerr black hole in a uniform Bertotti-Robinson magnetic field: An exact solution,” *arXiv preprint arXiv:2507.05199* (2025) .
- [46] B. Bertotti, “Uniform electromagnetic field in the theory of general relativity,” *Phys. Rev.* **116** (Dec,

- 1959) 1331–1333. <https://link.aps.org/doi/10.1103/PhysRev.116.1331>.
- [47] I. Robinson, “A solution of the maxwell-einstein equations,” *Bulletin de l’Académie Polonaise des Sciences. Série des Sciences Mathématiques, Astronomiques et Physiques* **7** (1959) 351–352.
- [48] L. Hu, R.-G. Cai, and S.-J. Wang, “Thermodynamics of Kerr-Bertotti-Robinson black hole,” [arXiv:2603.18821 \[gr-qc\]](https://arxiv.org/abs/2603.18821).
- [49] M. Abramowitz and I. A. Stegun, *Handbook of mathematical functions with formulas, graphs, and mathematical tables*, vol. 55. US Government printing office, 1964.
- [50] C. M. Bender and S. A. Orszag, *Advanced mathematical methods for scientists and engineers I: Asymptotic methods and perturbation theory*. Springer Science & Business Media, 1999.
- [51] W. H. Press, S. A. Teukolsky, W. T. Vetterling, and B. P. Flannery, *Numerical recipes 3rd edition: The art of scientific computing*. Cambridge university press, 2007.
- [52] J. M. Bardeen, W. H. Press, and S. A. Teukolsky, “Rotating black holes: locally nonrotating frames, energy extraction, and scalar synchrotron radiation,” *The Astrophysical Journal* **178** (1972) 347–370.
- [53] D. V. Galtsov and V. I. Petukhov, “Black Hole in an External Magnetic Field,” *Zh. Eksp. Teor. Fiz.* **74** (1978) 801–818.
- [54] S.-J. Zhang, “Energy extraction via magnetic reconnection in magnetized black holes,” *arXiv preprint arXiv:2405.16941* (2024) .
- [55] R. C. Duncan, “Physics in ultra-strong magnetic fields,” *AIP Conf. Proc.* **526** no. 1, (2000) 830, [arXiv:astro-ph/0002442](https://arxiv.org/abs/astro-ph/0002442).